

# Preferential Siting of Aluminum Heteroatoms in the Zeolite Catalyst Al-SSZ-70

Zachariah J. Berkson, Ming-Feng Hsieh, Stef Smeets, David Gajan, Alicia Lund, Anne Lesage, Dan Xie, Stacey I. Zones, Lynne B. McCusker, Christian Baerlocher, and Bradley F. Chmelka\*

**Abstract:** The adsorption and reaction properties of heterogeneous zeolite catalysts (e.g. for catalytic cracking of petroleum, partial oxidation of natural gas) depend strongly on the types and distributions of Al heteroatoms in the aluminosilicate frameworks. The origins of these properties have been challenging to discern, owing in part to the structural complexity of aluminosilicate zeolites. Herein, combined solid-state NMR and synchrotron X-ray powder diffraction analyses show the Al atoms locate preferentially in certain framework sites in the zeolite catalyst Al-SSZ-70. Through-covalent-bond 2D  $^{27}\text{Al}|^{29}\text{Si}$  J-correlation NMR spectra allow distinct framework Al sites to be identified and their relative occupancies quantified. The analyses show that 94% of the Al atoms are located at the surfaces of the large-pore interlayer channels of Al-SSZ-70, while only 6% are in the sub-nm intralayer channels. The selective siting of Al atoms accounts for the reaction properties of catalysts derived from SSZ-70.

Nanoporous zeolites are of considerable technological interest because of their high surface areas, well-defined sub-nanometer pore dimensions, and exchangeable cations.<sup>[1]</sup>

Their molecular adsorption or reaction sites enable important industrial applications, including air–gas separations<sup>[2]</sup> and heterogeneous catalysis of reactions such as hydrocarbon conversions<sup>[3]</sup> and reduction of nitric oxides for automotive pollution mitigation.<sup>[4]</sup> Aluminosilicate zeolites are composed of corner-sharing  $\text{SiO}_4$  and  $\text{AlO}_4$  tetrahedra, where the  $\text{AlO}_4$  tetrahedra are associated with catalytically active sites when the excess negative framework charges are balanced by acidic counterocations, such as  $\text{H}^+$ . The molecular diffusion, adsorption, and reaction properties of zeolite catalysts are strongly influenced by the nanopore dimensions, the framework architectures, and the types and distributions of heteroatom sites (e.g. Al) and the associated cations. Understanding and controlling heteroatom locations in zeolite catalysts have been severely limited by the non-stoichiometric substitution of heteroatoms into the framework and their distributions, which are challenging to characterize. Determining such distributions in different zeolite frameworks and correlating their macroscopic adsorption and/or catalytic reaction properties has been a long-standing challenge in the understanding of zeolite catalysts.

Heteroatom distributions in zeolites have long been recognized to depend strongly on synthesis conditions, including the compositions of the precursor materials and organic and inorganic structure-directing cations.<sup>[5]</sup> Information on heteroatom distributions in zeolites has been accessed previously by using several scattering or spectroscopic techniques. For example, the relative positions and proximities of Al atoms and their associated cations may be identified by deconvolution of infrared or ultraviolet-visible spectra of zeolite frameworks,<sup>[6–8]</sup> though such spectra are generally poorly resolved. While the similar electron densities of Al and Si atoms make them challenging to distinguish using scattering techniques,<sup>[9]</sup> Al occupancies in different tetrahedral (T) sites have been determined for large single crystals by synchrotron X-ray standing-wave diffraction.<sup>[10]</sup> For as-synthesized zeolites containing organic structure-directing agents (OSDAs) that drive preferential configurations of heteroatom sites, information on framework heteroatom distributions may be extracted by the refinement of synchrotron X-ray diffraction data.<sup>[11–13]</sup> Heteroatom distributions in zeolites can be influenced in favorable cases by the substitution of Al for B<sup>[14]</sup> or the careful selection of OSDAs and synthesis conditions.<sup>[11,15–17]</sup>

Herein, analyses of solid-state two-dimensional (2D) NMR spectra with complementary synchrotron X-ray powder diffraction analyses establish the preferential siting of Al heteroatoms in calcined zeolite Al-SSZ-70. The layered zeolite SSZ-70 has recently emerged as a promising platform

[\*] Dr. Z. J. Berkson, Dr. M.-F. Hsieh, Dr. L. B. McCusker, Dr. C. Baerlocher, Prof. Dr. B. F. Chmelka  
Department of Chemical Engineering  
University of California  
Santa Barbara, CA 93106 (USA)  
E-mail: bradc@engineering.ucsb.edu

Dr. S. Smeets, Dr. L. B. McCusker, Dr. C. Baerlocher  
Laboratory of Crystallography, ETH Zurich  
Vladimir-Prelog-Weg 5, 8093 Zurich (Switzerland)


Dr. D. Gajan, Dr. A. Lund, Dr. A. Lesage  
Institut des Sciences Analytiques UMR 5280 (CNRS/Université Lyon 1/ENS Lyon), Université Lyon, Centre de RMN à Très Hauts Champs  
69100 Villeurbanne (France)

Dr. D. Xie, Dr. S. I. Zones  
Chevron Energy Technology Company  
Richmond, CA 94802 (USA)

Dr. M.-F. Hsieh  
Present address: Johnson Matthey Technology Centre  
Chilton P.O. Box 1, Belasis Avenue, Billingham TS23 1LB (UK)

Dr. S. Smeets  
Present address: Kavli Institute of Nanoscience, Delft University of Technology

Van der Maasweg 9, 2629 HZ Delft (The Netherlands)

 Supporting information (experimental details, 2D  $^{27}\text{Al}$  MQMAS analyses, 1D  $^{27}\text{Al}$  and  $^{29}\text{Si}$  NMR spectra, NMR sensitivity enhancement under low-temperature conditions, additional discussion) and the ORCID identification number(s) for the author(s) of this article can be found under:

<https://doi.org/10.1002/anie.201813533>.

for new catalysts because it can be exfoliated to generate high-surface-area active materials that exhibit enhanced catalysis rates for alkylation reactions,<sup>[18]</sup> while calcined Al-SSZ-70 exhibits high catalytic activity for hydrocarbon cracking.<sup>[19]</sup> The structure of calcined SSZ-70 has 14 crystallographically distinct T sites.<sup>[20]</sup> SSZ-70 crystallizes into hexagonal flakes (Figure 1a) and has two types of 2-dimensional

indicating that the long-range ordering of T-atoms in SSZ-70 is indistinguishable in silicate and aluminosilicate forms, despite their different compositions.

Analyses of the 1D <sup>29</sup>Si MAS NMR spectra (Figure S1 in the Supporting Information) show that the local environments of framework <sup>29</sup>Si atoms in calcined SSZ-70 are almost identical in the siliceous and aluminosilicate forms. Because of the small absolute quantity of Al in the material (Si/Al = 25, Ref. [19]) and overlapping <sup>29</sup>Si NMR signals from different *Q*<sup>4</sup>(0Al) and *Q*<sup>3</sup>(0Al) species in SSZ-70,<sup>[20]</sup> the <sup>29</sup>Si signals from *Q*<sup>4</sup>(1Al) species cannot be resolved or quantified from the 1D <sup>29</sup>Si MAS NMR spectra alone. (The *Q*<sup>*m*</sup>(*n*Al) notation refers to a tetrahedrally coordinated <sup>29</sup>Si atom that is covalently linked through bridging O atoms to *m* other Si or Al atoms, of which *n* are Al.)

Solid-state <sup>27</sup>Al NMR spectroscopy is sensitive to the local environments of the crucial Al heteroatoms in zeolite frameworks and is in principle capable of distinguishing between <sup>27</sup>Al species in different T sites in aluminosilicate zeolites.<sup>[22]</sup> However, the resolution of such spectra is often limited owing to strong quadrupolar interactions of <sup>27</sup>Al (*I* = 5/2) nuclei, as well as inhomogeneous distributions of <sup>27</sup>Al species. The resolution of solid-state <sup>27</sup>Al NMR spectra can be improved by using high magnetic fields (> 18 Tesla) and 2D NMR techniques.<sup>[23]</sup> For example, high-field <sup>27</sup>Al multiple-quantum magic-angle-spinning (MQMAS) NMR analyses of different samples of aluminosilicate zeolite ZSM-5, which has 24 crystallographically distinct T sites, have led to the identification and assignment of at least 12 different <sup>27</sup>Al signals associated with different T sites.<sup>[24–26]</sup> In addition, recent 2D <sup>27</sup>Al{<sup>29</sup>Si} dipolar-mediated NMR analyses of ZSM-5 provided evidence of Al incorporation into 4 of the 24 T sites,<sup>[27]</sup> although through-space dipolar interactions can manifest signal intensities from next-nearest neighbor T sites and non-covalently bonded moieties that reduce resolution. General methods for determining the distributions and relative populations of Al heteroatoms in zeolites have been elusive, particularly for materials of high catalytic importance that often exhibit exceptional structural complexity, such as Al-SSZ-70.

Herein, we report the preferential siting of Al heteroatoms in 5 of the 14 T sites in calcined Al-SSZ-70 established by analyses of solid-state 2D NMR heteronuclear correlation spectra,<sup>[27,28]</sup> which resolve distinct signals from different framework <sup>27</sup>Al moieties and provide direct evidence for the incorporation of Al atoms into specific sites. The 1D and 2D <sup>27</sup>Al MAS NMR spectra of calcined Al-SSZ-70 in Figure 2 show well-resolved <sup>27</sup>Al signals at 60 ppm, 55 ppm, and 49 ppm from <sup>27</sup>Al atoms in tetrahedrally coordinated environments, as well as a signal at –5 ppm from octahedrally coordinated <sup>27</sup>Al species. The relatively narrow (2–3 ppm full-width half-maximum, fwhm) <sup>27</sup>Al signals suggest that the <sup>27</sup>Al heteroatoms are sited in specific T sites, rather than being randomly distributed.

Specific locations of Al heteroatoms in calcined Al-SSZ-70 are determined by identification of the nearest-neighbor <sup>29</sup>Si sites to which the different <sup>27</sup>Al species are covalently bonded. This is achieved by measuring 2D <sup>27</sup>Al{<sup>29</sup>Si} heteronuclear multiple quantum correlation (HMQC) NMR spectra,<sup>[29–31]</sup> which here correlate the shifts of <sup>27</sup>Al–O–<sup>29</sup>Si spin

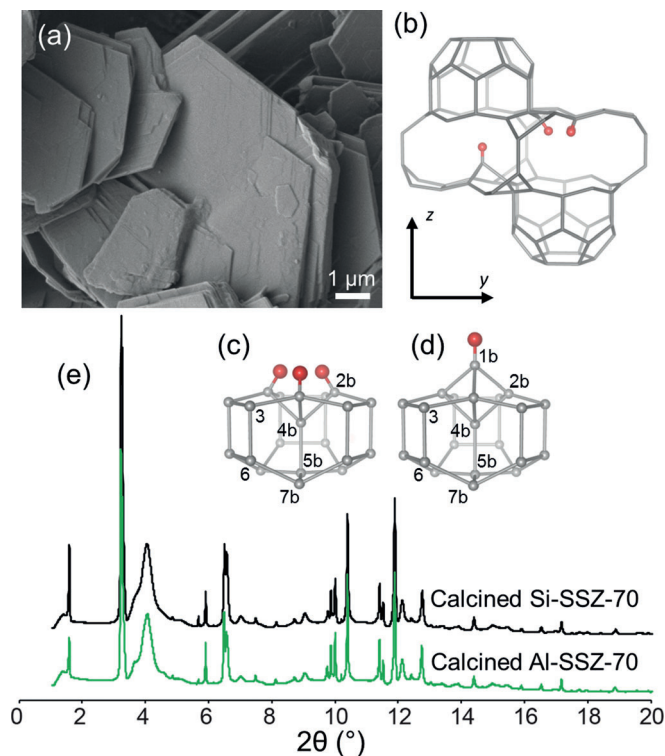


**Figure 1.** a) SEM image of Al-SSZ-70. b) Interlayer structure of calcined SSZ-70, showing the two types of interlayer -OH species (red; (c,d)). e) Synchrotron XRPD patterns of calcined Si- (black) and Al-SSZ-70 (green).

channel systems with effective cross-sectional pore openings of  $4.4 \times 5.9 \text{ \AA}^2$  (within the **MWW**-type layers) and  $4.0 \times 11.5 \text{ \AA}^2$  (between the **MWW**-type layers). However, in contrast to other **MWW**-type zeolite catalysts, the catalytic selectivity of calcined Al-SSZ-70 for hydrocarbon cracking does not change substantially with time on stream,<sup>[19]</sup> characteristic of reactions occurring in a single type of nanochannel system.<sup>[21]</sup> Calcined SSZ-70 exhibits two types of silanol species that protrude into the interlayer channels (Figure 1b): “nests” of three closely spaced silanols (Figure 1c) and isolated silanols (Figure 1d). The different T sites in SSZ-70 differ with respect to their covalent bonding configurations and positions relative to the inter- and intralayer channel surfaces. For example, T1a,b, T2a,b, and T3 are at the surfaces of the interlayer channels, while T5a,b, T6, T7a,b, and T8a,b are at the surfaces of the intralayer channels. Al heteroatoms located in such different T sites are expected to exhibit distinct adsorption and reaction properties. The synchrotron X-ray powder diffraction (XRPD) patterns of calcined Si- and Al-SSZ-70 are virtually identical (Figure 1e),

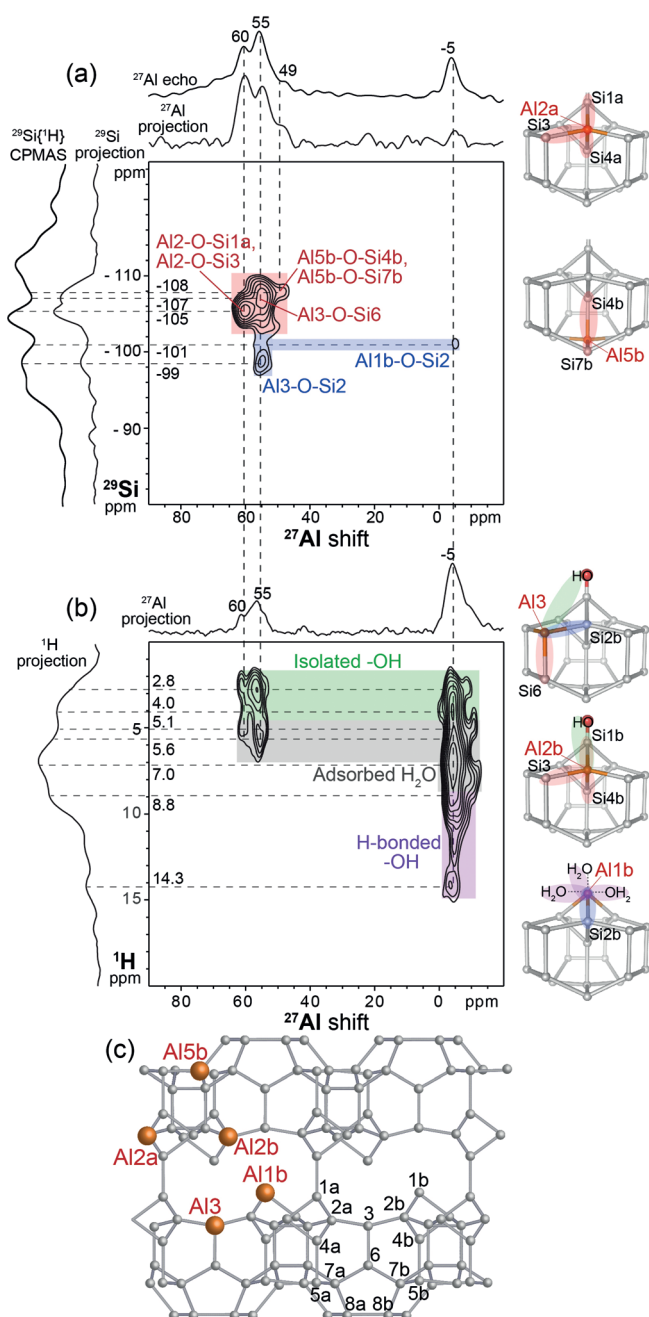


**Figure 2.** Solid-state 2D a)  $^{27}\text{Al}\{^{29}\text{Si}\}$   $J$ -HMQC and b)  $^{27}\text{Al}\{^1\text{H}\}$  HETCOR NMR spectra of calcined Al-SSZ-70 acquired at 18.8 Tesla, 10 kHz MAS, and 97 K. Solid-state 1D  $^{27}\text{Al}$  echo and  $^{29}\text{Si}\{^1\text{H}\}$  CPMAS spectra acquired under the same conditions are shown along the corresponding axes for comparison with the 1D projections of the 2D spectra. The accompanying insets show the  $J$ -coupling between  $^{27}\text{Al}$  atoms (orange) and  $^{29}\text{Si}$  atoms (gray) at nearest-neighbor T sites consistent with the correlated intensities in the 2D spectra in (a) and (b). c) Schematic diagram of the framework structure of Al-SSZ-70, with orange indicating the T sites that are occupied by Al heteroatoms as determined by the solid-state NMR analyses.

pairs and are mediated by through-covalent-bond  $J_{\text{Al-Si}}$  couplings.<sup>[32]</sup> Acquisition of such spectra has been exceptionally challenging in the past, but is enabled here by the use of low-temperature (< 100 K) measurement conditions, which

lead to improved NMR signal sensitivity (ca.  $5 \times$  increase) (Figure S2, S3). For example, the 2D  $^{27}\text{Al}\{^{29}\text{Si}\}$   $J$ -HMQC spectrum of calcined Al-SSZ-70 in Figure 2a shows correlated signal intensities at  $^{27}\text{Al}$  shifts of 60 ppm, 55 ppm, and 49 ppm that are correlated with  $^{29}\text{Si}$  signals in the chemical shift range  $-105$  ppm to  $-108$  ppm (red band in Figure 2a) from different  $Q^4(1\text{Al})$   $^{29}\text{Si}$  species. The  $^{27}\text{Al}$  signal at 55 ppm is additionally correlated with  $^{29}\text{Si}$  signals in the  $-99$  to  $-101$  ppm range (blue band), which also arise from  $Q^4(1\text{Al})$  species. The different correlated  $^{27}\text{Al}$ - $^{29}\text{Si}$  signals in the 2D  $^{27}\text{Al}\{^{29}\text{Si}\}$   $J$ -mediated spectrum in Figure 2a are assigned based on comparisons with previous 2D  $^{29}\text{Si}\{^{29}\text{Si}\}$  and  $^{29}\text{Si}\{^1\text{H}\}$  NMR analyses of calcined Si-SSZ-70,<sup>[20]</sup> analyses of 2D  $^{27}\text{Al}$  MQMAS spectra of Al-SSZ-70 (Figures S4, S5, Tables S1, S2), well-established semi-empirical correlations relating the isotropic  $^{27}\text{Al}$  and  $^{29}\text{Si}$  chemical shift values to the  $-\text{T}-\text{O}-\text{T}-$  bond angles,<sup>[33–35]</sup> and prior literature.<sup>[36]</sup> The predicted and experimental isotropic  $^{27}\text{Al}$  and  $^{29}\text{Si}$  chemical shifts associated with different T sites in calcined Al-SSZ-70 are compared in Figure S6. On the basis of isotropic  $^{29}\text{Si}$  chemical shift values calculated for  $Q^4(1\text{Al})$  species in each T site (Table S3), the correlated signals at  $-99$  to  $-101$  ppm in the  $^{29}\text{Si}$  dimension (blue band in Figure 2a) are assigned to framework Al-O-Si2  $Q^4(1\text{Al})$  moieties, while those at  $-105$ ,  $-107$ , and  $-108$  ppm (red band; Figure 2a) are assigned, respectively, to Al-O-Si3 and Al-O-Si1a, Al-O-Si6, and Al-O-Si4b and Al-O-Si7b  $Q^4(1\text{Al})$  moieties. The correlated  $^{27}\text{Al}$ - $^{29}\text{Si}$  signals at 60, 55, and 49 ppm in the  $^{27}\text{Al}$  dimension must therefore arise from  $^{27}\text{Al}$  species that are covalently bonded (through bridging O atoms) to Si1a and Si3, Si6 and Si2, and Si4b and Si7b  $Q^4(1\text{Al})$  species, respectively. The positions of the  $^{27}\text{Al}$  heteroatoms are further constrained by analysis of the isotropic  $^{27}\text{Al}$  chemical shifts determined by 2D  $^{27}\text{Al}$  MQMAS analyses at different magnetic field strengths and temperatures (Figures S4, S5), which are compared with the calculated values for  $^{27}\text{Al}$  atoms in each T site (Table S2, Figure S6). With the constraints provided by the 2D  $^{27}\text{Al}\{^{29}\text{Si}\}$   $J$ -mediated correlation spectrum, these analyses enable the  $^{27}\text{Al}$  signals at 60, 55, and 49 ppm to be confidently assigned to fully crosslinked Al2a/b, Al3, and Al5b sites, respectively. The unambiguous identification of the different  $^{27}\text{Al}$ -O- $^{29}\text{Si}$  connectivities enables the specific locations of Al heteroatoms to be established, even for a complex zeolite, such as Al-SSZ-70.

Interestingly, octahedrally coordinated  $^{27}\text{Al}$  species are also located within the aluminosilicate zeolite framework. Octahedrally coordinated framework  $^{27}\text{Al}$  species in aluminosilicate zeolites are generally associated with framework defect sites and/or partial dealumination of the framework.<sup>[37]</sup> The correlation of the  $^{29}\text{Si}$  signal at  $-101$  ppm from Si2  $Q^4(1\text{Al})$  species and the  $^{27}\text{Al}$  signal at  $-5$  ppm (blue band, Figure 2a) establishes that the octahedrally coordinated  $^{27}\text{Al}$  species in Al-SSZ-70 are in fact covalently linked to Si2  $Q^4(1\text{Al})$  species and are therefore in T1a/b or T3 sites. The presence of this weak correlated signal is confirmed by the 2D  $^{27}\text{Al}\{^{29}\text{Si}\}$   $J$ -HMQC spectrum acquired at 9.4 Tesla and 91 K (Figure S7). Because of steric hindrance near framework T1a and T3 sites, the presence of octahedrally coordinated Al1a or Al3 species is considered unlikely. By comparison, T1b is a partially crosslinked site that protrudes into the interlayer



channels, where  $^{27}\text{Al}$  atoms could coordinate to adsorbed water and/or -OH groups. Octahedrally coordinated Al1b species are therefore expected to be associated with significant hydrogen bonding.

Strong H-bonds associated with the octahedrally coordinated  $^{27}\text{Al}$  species in calcined Al-SSZ-70 are identified by analysis of the 2D  $^{27}\text{Al}\{^1\text{H}\}$  heteronuclear correlation (HETCOR) spectrum of calcined Al-SSZ-70 (Figure 2b). The spectrum manifests correlated  $^{27}\text{Al}\{^1\text{H}\}$  signal intensities from  $^{27}\text{Al}$ - $^1\text{H}$  nuclear spin pairs that are dipole-dipole coupled through space, being principally sensitive to interactions over distances of  $< 5 \text{ \AA}$ .<sup>[38]</sup> Analyses of 1D  $^1\text{H}$  and 2D  $^{29}\text{Si}\{^1\text{H}\}$  HETCOR NMR spectra of calcined Si- and Al-SSZ-70 (Figures S3, S8) show that both materials possess isolated and strongly H-bonded interlayer -OH species. The 2D  $^{27}\text{Al}\{^1\text{H}\}$  HETCOR spectrum of calcined Al-SSZ-70 in Figure 2b shows correlated intensities at 55 and 60 ppm in the  $^{27}\text{Al}$  dimension and at 2.8–4.0 ppm (green band, Figure 2b) and 5.1–5.6 ppm (gray band, Figure 2b) in the  $^1\text{H}$  dimension, which arise from tetrahedrally coordinated  $^{27}\text{Al}$  species proximate to isolated interlayer -OH groups<sup>[20]</sup> and nanopore-adsorbed water,<sup>[39]</sup> respectively. These signals are consistent with the assignment of the  $^{27}\text{Al}$  signals at 55 and 60 ppm to fully crosslinked Al2a/b and Al3 sites, respectively. By comparison, the  $^{27}\text{Al}$  signal at  $-5 \text{ ppm}$  is correlated with a broad, continuous distribution of  $^1\text{H}$  signals from 2.8–14.3 ppm. The  $^1\text{H}$  signals at 2.8–4.0 ppm (green band, Figure 2b) are assigned to isolated -OH species, those at 5.1–7.0 ppm (gray band, Figure 2b) to adsorbed water molecules, and those at 8.8–14.3 ppm (purple band, Figure 2b) to H-bonded -OH groups with -OH $\cdots$ O- distances of 2.5 Å to 2.8 Å as estimated from well-established semi-empirical correlations.<sup>[39,40]</sup> The correlated  $^{27}\text{Al}\{^1\text{H}\}$  signal intensities thus establish that the octahedrally coordinated  $^{27}\text{Al}$  species are in close proximities to isolated and strongly H-bonded -OH moieties. All of the solid-state NMR results are therefore consistent with the assignment of the  $^{27}\text{Al}$  signal at  $-5 \text{ ppm}$  to partially crosslinked Al1b sites, which are bonded (through bridging oxygen atoms) to three framework Si atoms and protrude into the interlayer channels, where Al atoms are able to adopt octahedral configurations by coordinating with water molecules or -OH groups.

Notably, the majority of the Al heteroatoms in calcined Al-SSZ-70 are located in framework sites at the surfaces of the interlayer channels. Based on the analyses of the solid-state 2D NMR spectra, each of the  $^{27}\text{Al}$  signals can be assigned with confidence to an individual T site within the zeolite Al-SSZ-70 framework structure. Specifically, the  $^{27}\text{Al}$  signals at 60, 55, and 49 ppm are assigned to  $^{27}\text{Al}$  atoms in fully crosslinked T-sites 2a/b, 3, and 5b, respectively, while the  $^{27}\text{Al}$  signal at  $-5 \text{ ppm}$  is assigned to octahedrally coordinated  $^{27}\text{Al}$  atoms in T-site 1b. Importantly, the relative occupancies of the  $^{27}\text{Al}$  heteroatoms in these different SSZ-70 framework sites are not the same. In fact, they are very different. Their relative populations are quantified by deconvolution of the 1D single-pulse  $^{27}\text{Al}$  spectrum (Figure S9), yielding the fractional occupancies of Al atoms in each of the five T sites (Table S4) that are shown in the schematic structure of calcined Al-SSZ-70 (Figure 2c). The great majority of the

$^{27}\text{Al}$  species (94%) are in T2a/b, T3, or T1b sites, which are located at the surfaces of the interlayer channels. The remainder of the  $^{27}\text{Al}$  species (6%) are at T5b sites, which are located at the surfaces of the intralayer channels.

Because of the different positions and local structures of Al atoms within the SSZ-70 framework, the different heteroatom sites are expected to influence the catalyst adsorption and reaction properties. The catalytic cracking of long-chain alkanes by Al-SSZ-70 is characteristic of a large-pore zeolite<sup>[19]</sup> rather than one with both large- and medium-pore channel systems, as might be expected from the structure of the zeolite. This is fully consistent with the preferential siting of Al heteroatoms at the surfaces of the large-pore interlayer channels, and indicates that the catalytic cracking (and probably other) reactions occur primarily there. The results also account for the high catalytic activities of catalysts derived from delamination of SSZ-70:<sup>[18,41]</sup> nearly all of the heteroatoms associated with the cation-exchange sites in Al-SSZ-70 are at the surfaces of the interlayer channels that are exposed upon exfoliation and therefore are accessible for post-synthetic modification and/or catalysis.

The locations of the majority of the Al heteroatoms at sites at the surfaces of the interlayer channels indicate that the bulky *N,N'*-diisobutylimidazolium cations used as OSDAs during zeolite synthesis direct the Al heteroatoms to specific sites in the Al-SSZ-70 framework. The roles of the OSDA in the preferential siting of Al heteroatoms in Al-SSZ-70 remain under investigation. In addition, the above analyses are expected to be useful for further studies on the structures of as-synthesized Al-SSZ-70 (Figure S10).

More broadly, recent research in zeolite materials has focused on generating active sites in specific regions of zeolites by designing zeolite architectures for specific reactions<sup>[16]</sup> or directing heteroatoms to targeted locations within a zeolite framework.<sup>[42]</sup> Such control over heteroatom locations is achievable in part for borosilicate zeolites by changing the OSDA and synthesis conditions.<sup>[13]</sup> However, similar capabilities have been lacking for aluminosilicate zeolites, in part because of the absence of experimental techniques that are capable of resolving Al occupancies at different T sites. The results reported here demonstrate that solid-state 2D NMR analyses, in combination with synchrotron XRPD, can establish Al locations and occupancies in complicated aluminosilicate zeolite frameworks like SSZ-70. This opens prospects for adjusting the Al distribution, and correspondingly the catalytic properties, by judicious selection of OSDAs and zeolite synthesis conditions.

In summary, the preferential siting of Al heteroatoms at 5 of the 14 T sites in calcined Al-SSZ-70 has been established by using 2D  $^{27}\text{Al}\{^{29}\text{Si}\}$  and  $^{27}\text{Al}\{^1\text{H}\}$  NMR correlation spectra to determine the T-site connectivities and hydration environments of specific  $^{27}\text{Al}$  sites. The analyses show that the majority of Al heteroatoms in Al-SSZ-70 are located at the surfaces of the interlayer channel regions, which are expected to strongly influence the adsorption and catalytic reaction properties of the material. Such insights provide a deeper atomic-level understanding of the adsorption and reaction properties of this emerging catalytic material. The approach used is general and can be expected to provide similar

understanding for other heteroatom-containing zeolite catalysts, aiding in the future design of new catalytic materials with improved activity, selectivity, and stability.

### Acknowledgements

This work was supported in part by the Chevron Energy Technology Company (Richmond, California, USA). The solid-state MAS NMR measurements at the University of California, Santa Barbara (UCSB), made use of the shared facilities of the UCSB MRL, supported by the MRSEC program of the NSF under Award No. DMR 1720256. Z.J.B. and B.F.C. thank the TGIR-RMN-THC Fr3050 CNRS for access to the 18.8 T DNP NMR facility at the CRMN and financial support was received from the EQUIPEX contract ANR-10-EQPX-47-01. S.S. acknowledges the Swiss National Science Foundation (Award No. 177761). We thank Drs. A. Cervellino and N. Casati for their assistance with the powder diffraction measurements on the Materials Science Beamline at the Swiss Light Source in Villigen, Switzerland.

### Conflict of interest

The authors declare no conflict of interest.

**Keywords:** aluminum · NMR spectroscopy · solid acids · zeolites

- [1] W. J. Roth, et al., *Nat. Chem.* **2013**, *5*, 628–633.
- [2] B. Wang, A. P. Côté, H. Furukawa, M. O’Keeffe, O. M. Yaghi, *Nature* **2008**, *453*, 207–211.
- [3] E. T. C. Vogt, B. M. Weckhuysen, *Chem. Soc. Rev.* **2015**, *44*, 7342–7370.
- [4] C. Paolucci, et al., *Science* **2017**, *357*, 898–903.
- [5] V. Gábová, J. Dědeček, J. Čejka, *Chem. Commun.* **2003**, 1196–1197.
- [6] J. Dědeček, D. Kaucký, B. Wichterlová, O. Gonsiorová, *Phys. Chem. Chem. Phys.* **2002**, *4*, 5406–5413.
- [7] R. Gounder, E. Iglesia, *J. Am. Chem. Soc.* **2009**, *131*, 1958–1971.
- [8] J. Hun Kwak, H. Zhu, J. H. Lee, C. H. F. Peden, J. Szanyi, *Chem. Commun.* **2012**, *48*, 4758.
- [9] J. Dědeček, Z. Sobalík, B. Wichterlová, *Catal. Rev. Sci. Eng.* **2012**, *54*, 135–223.
- [10] J. A. van Bokhoven, T. L. Lee, M. Drakopoulos, C. Lamberti, S. Thie, J. Zegenhagen, *Nat. Mater.* **2008**, *7*, 551–555.
- [11] A. B. Pinar, L. Gómez-Hortigüela, L. B. McCusker, J. Pérez-Pariente, *Chem. Mater.* **2013**, *25*, 3654–3661.
- [12] S. Smeets, L. B. McCusker, C. Baerlocher, D. Xie, C. Y. Chen, S. I. Zones, *J. Am. Chem. Soc.* **2015**, *137*, 2015–2020.
- [13] S. Smeets, L. B. McCusker, C. Baerlocher, S. Elomari, D. Xie, S. I. Zones, *J. Am. Chem. Soc.* **2016**, *138*, 7099–7106.
- [14] S. I. Zones, A. Benin, S.-J. Hwang, D. Xie, S. Elomari, M.-F. Hsieh, *J. Am. Chem. Soc.* **2014**, *136*, 1462–1471.
- [15] J. R. Di Iorio, C. T. Nimlos, R. Gounder, *ACS Catal.* **2017**, *7*, 6663–6674.
- [16] E. M. Gallego, M. T. Portilla, C. Paris, A. León-Escamilla, M. Boronat, M. Moliner, A. Corma, *Science* **2017**, *355*, 1051–1054.
- [17] K. Muraoka, W. Chaikittisilp, Y. Yanaba, T. Yoshikawa, T. Okubo, *Angew. Chem. Int. Ed.* **2018**, *57*, 3742–3746; *Angew. Chem.* **2018**, *130*, 3804–3808.
- [18] R. C. Runnebaum, X. Ouyang, J. A. Edsinga, T. Rea, I. Arslan, S.-J. J. Hwang, S. I. Zones, A. Katz, *ACS Catal.* **2014**, *4*, 2364–2368.
- [19] R. H. Archer, J. R. Carpenter, S.-J. Hwang, A. W. Burton, C.-Y. Chen, S. I. Zones, M. E. Davis, *Chem. Mater.* **2010**, *22*, 2563–2572.
- [20] S. Smeets, Z. J. Berkson, D. Xie, S. I. Zones, W. Wan, X. Zou, M. F. Hsieh, B. F. Chmelka, L. B. McCusker, C. Baerlocher, *J. Am. Chem. Soc.* **2017**, *139*, 16803–16812.
- [21] S. I. Zones, T. V. Harris, *Microporous Mesoporous Mater.* **2000**, *35–36*, 31–46.
- [22] M. Haouas, F. Taulelle, C. Martineau, *Prog. Nucl. Magn. Reson. Spectrosc.* **2016**, *94–95*, 11–36.
- [23] L. Frydman, D. M. Grant, R. K. Harris, *Encycl. Nucl. Magn. Reson.* **2002**, *9*, 262–274.
- [24] S. Sklenak, J. Dědeček, C. Li, B. Wichterlová, V. Gábová, M. Sierka, J. Sauer, *Angew. Chem. Int. Ed.* **2007**, *46*, 7286–7289; *Angew. Chem.* **2007**, *119*, 7424–7427.
- [25] S. Sklenak, J. Dědeček, C. Li, B. Wichterlová, V. Gábová, M. Sierka, J. Sauer, *Phys. Chem. Chem. Phys.* **2009**, *11*, 1237–1247.
- [26] J. Holzinger, P. Beato, L. F. Lundegaard, J. Skibsted, *J. Phys. Chem. C* **2018**, *122*, 15595–15613.
- [27] E. Dib, T. Mineva, E. Veron, V. Sarou-Kanian, F. Fayon, B. Alonso, *J. Phys. Chem. Lett.* **2018**, *9*, 19–24.
- [28] A. G. M. Rankin, P. B. Webb, D. M. Dawson, J. Viger-Gravel, B. J. Walder, L. Emsley, S. E. Ashbrook, *J. Phys. Chem. C* **2017**, *121*, 22977–22984.
- [29] A. Lesage, D. Sakellariou, S. Steuernagel, L. Emsley, *J. Am. Chem. Soc.* **1998**, *120*, 13194–13201.
- [30] P. Florian, E. Veron, T. F. G. Green, J. R. Yates, D. Massiot, *Chem. Mater.* **2012**, *24*, 4068–4079.
- [31] M. Valla, et al., *J. Am. Chem. Soc.* **2015**, *137*, 10710–10719.
- [32] D. Massiot, et al., *C. R. Chim.* **2010**, *13*, 117–129.
- [33] S. Ramdas, J. Klinowski, *Nature* **1984**, *308*, 521–523.
- [34] E. Lippmaa, A. Samoson, M. Magi, *J. Am. Chem. Soc.* **1986**, *108*, 1730–1735.
- [35] D. M. Dawson, R. F. Moran, S. E. Ashbrook, *J. Phys. Chem. C* **2017**, *121*, 15198–15210.
- [36] M. A. Camblor, A. Corma, M.-J. Díaz-Cabañas, C. Baerlocher, *J. Phys. Chem. B* **1998**, *102*, 44–51.
- [37] A. Omega, J. A. van Bokhoven, R. Prins, *J. Phys. Chem. B* **2003**, *107*, 8854–8860.
- [38] M. T. Janicke, C. C. Landry, S. C. Christiansen, D. Kumar, G. D. Stucky, B. F. Chmelka, *J. Am. Chem. Soc.* **1998**, *120*, 6940–6951.
- [39] J. P. Yesinowski, H. Eckert, G. R. Rossman, *J. Am. Chem. Soc.* **1988**, *110*, 1367–1375.
- [40] X. Xue, M. Kanzaki, *J. Am. Ceram. Soc.* **2009**, *92*, 2803–2830.
- [41] M. Aigner, N. A. Grosso-Giordano, A. Okrut, S. Zones, A. Katz, *React. Chem. Eng.* **2017**, *2*, 842–851.
- [42] S. I. Zones, C. Y. Chen, A. Benin, S.-J. Hwang, *J. Catal.* **2013**, *308*, 213–225.

Manuscript received: November 27, 2018

Version of record online: ■■■■■, ■■■■■

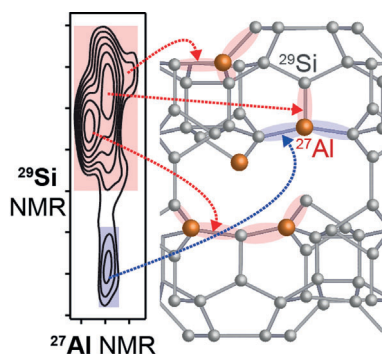
## Zuschriften



## Zeolithe

Z. J. Berkson, M.-F. Hsieh, S. Smeets,  
D. Gajan, A. Lund, A. Lesage, D. Xie,  
S. I. Zones, L. B. McCusker, C. Baerlocher,  
B. F. Chmelka\* ————— ■■■■-■■■■

Preferential Siting of Aluminum  
Heteroatoms in the Zeolite Catalyst Al-  
SSZ-70



**Al-Atome lokalisiert:** Die Adsorptions- und Reaktionenseigenschaften heterogener Zeolith-Katalysatoren hängen von der Verteilung der Al-Atome in den Aluminosilicat-Gerüsten ab. Die Positionen und Besetzungen von Al-Heteroatomen im Zeolith-Katalysator Al-SSZ-70 wurden durch Festkörper-NMR und Synchrotron-XRPD-Analysen bestimmt. Die selektive Positionierung der Al-Atome beeinflusst die Reaktionenseigenschaften der von SSZ-70 abgeleiteten Katalysatoren.